PROCEEDINGS OF SPIE

SPIEDigitalLibrary.org/conference-proceedings-of-spie

2DEG channel-dependent model for Hg_{1-x}Cd_x Te-based pseudomorphic HEMTs

Hang-Ming Dai
Thomas J. Sanders

SPIE.

A 2DEG Channel-Dependent Model for $Hg_{1-x}Cd_xTe$ Based Pseudomorphic HEMTs

Hung-Ming Dai and Thomas Sanders

Department of Electrical Engineering, Florida Institute of Technology

P.O. Box 61796, Palm Bay, FL 32906

email: hdai@usa.com

Abstract

HgCdTe has emerged as an important electronic material because of its IRFPA applications. Technologies for growing the material are advanced and current sources for the material are more readily available than in the past. This brings an advantage to the manufacturing other types of HgCdTe devices. PHEMTs are attractive as applications of high-speed devices. In this paper, a model for PHEMT devices by using $Hg_{1-x}Cd_xTe$ as device materials is presented. High digital performance of the device is expected because electron mobility of the material is very high at low temperatures.
Keywords: MCTS, PHEMT, 2DEG, HgCdTe, FEM, AAFEM

Introduction

Most HEMTs and PHEMTs are made of AlGaAs or InGaAs. Thus far, HgCdTe has not yet been used as a device material for HEMT devices. This material has been used for fabrication of IRFPA devices, and its significance has been increasing. In this paper, an HgCdTe based PHEMT device is presented. The device was modeled and calculated by using the finite element method. A computer program called MCTS (Mercury Cadmium Telluride Simulator) was developed to perform the computations. MCTS is driven by MCTA (MCT Assembly), which is a text based simulation language. To enhance user-friendly programming for the computer language, a GUI (Graphical User Interface) program called MCTG (MCT GUI) was also built for modern operating systems such as Windows. MCTS has been used for simulating HgCdTe IRFPA devices,[1-3] and the results have agreed with experimental data. Success of the simulation approaches provided an opportunity to probe innovative HgCdTe PHEMTs. Similar to other PHEMTs, quantum phenomena in 2DEG channel were also predicted in HgCdTe PHEMT. In this study, a new method was developed by proper modification of the channel parameters such as carrier mobilities, to improve computational accuracy.

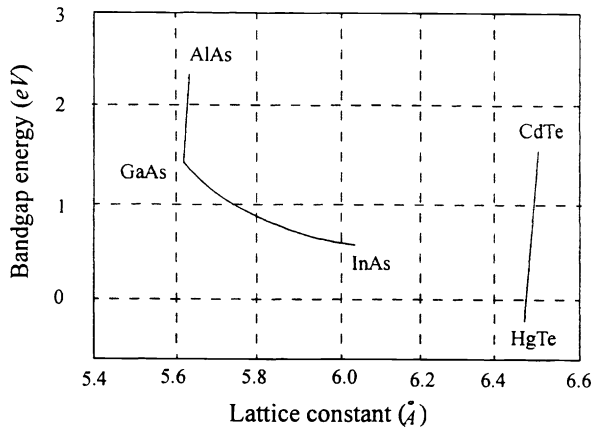

Figure 1 Bandgap energy vs. Lattice constant at room temperature

PHEMT is considered as an extension of HEMT by inducing a pseudomorphic layer as its conduction channel. It is also known to have lower g-r and 1/f noise than HEMT's of the same class.[4] PHEMTs posses properties of excellent high-speed, low-noise, and power applications.[5-7] Matthew and Blakeslee studied pseudomorphic layers and explained that these layers were strained to conform lattice mismatch.[8] When a layer thickness is less than a critical level, electron flows in the stained

In *Enabling Photonic Technologies for Aerospace Applications II*, Edward W. Taylor, Andrew R. Pirich, Editors, Proceedings of SPIE Vol. 4042 (2000) • 0277-786X/00/$15.00

layer are energetically promoted. HgCdTe is a ternary alloy. The material characteristics are associated with the Cd composition fraction: CdTe is a semiconductor whereas coloradoite is a semimetal. A plot of bandgap energy versus lattice constant for AlGaAs, InGaAs, and HgCdTe compounds are shown in Figure 1.[9,10]

Lattice mismatch between coloradoite and CdTe is $0.0147\mathring{A}$. In comparison with AlInAs, crystal strain of HgCdTe at a mechanical interface for different x is very low. Low lattice mismatch can improve crystal defects at epitaxial layers.[12]

Propagation delay (τ_d) is the minimum time required to switch on and off a transistor.[4] Carrier mobilities are important parameters that directly associated with τ_d. In a laboratory, electron mobility of $Hg_{0.80}Cd_{0.20}Te$ has been demonstrated as high as $3E5\,cm^2/Vs$ at $77°K$.[13] Intrinsic concentration of $Hg_{0.82}Cd_{0.18}Te$ is $1.0E15\,cm^{-3}$ at $80\ °K$. High carrier concentration in the 2DEG channel can result in carrier charge screening from an impurity field.[14] The low friction produced in the channel allows drift speed of electrons to approach high-field-saturation velocity.[15] Due to the crystal strain in the pseudomorphic layer, carrier concentration and electron mobility in 2DEG channel actually exceed their unstrained limits.[4] Observations from computer simulations recorded the electric field in the channel, as very high, thus greatly accelerating electrons. Speedy electrons in the channel and active layers hence caused significant reduction of τ_d. The enhanced electron mobility and concentration in a 2DEG channel favors transconductance, g_m which is a crucial parameter for small-signal analysis.

This paper is divided into eight sections. Section 1 is the Introduction. Section 2 contains the Device Structure for the model. Section 3 contains Device Equations for the model. Section 4 presents Simulation Results and Discussions. Section 5 is Applications for HgCdTe PHEMTs. Section 6 is Acknowledgments. Section 7 is References, and Section 8 shows Figures of the simulation results. Since PHEMT is considered as an extension of HEMT, analysis of PHEMTs is similar to HEMTs'.

Device Structure

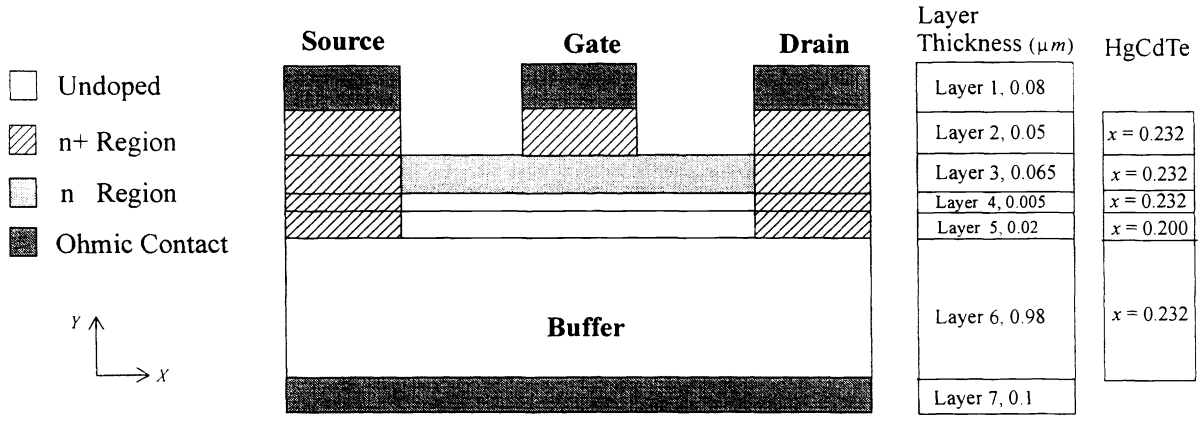

Figure 2 Schematic cross section of the HgCdTe PHEMT

Figure 2 shows the device structure. n+ region is doped with donor concentration $1.0E17\,cm^{-3}$. n region is doped with donor concentration $1.0E16\,cm^{-3}$. The device contacts are ohmic. The gate width is $0.15\,\mu m$ and the drain and source widths are $0.25\,\mu m$ each.

Device Equations

The following equations were used for modeling HgCdTe PHEMTs.

Poisson Equation

Electric field is governed by the Poisson equation, which is defined as [11]

$$\nabla \cdot \varepsilon_p \xi = \rho, \tag{1}$$

where ε_p is permittivity of HgCdTe, ξ is electric field, and ρ is total charge.

Current Equations

Electron current is defined as [11]

$$J_n = q(n\mu_n\xi + D_n\nabla n), \tag{2}$$

where q is unit charge, μ_n is electron mobility, D_n is electron diffusion coefficient, n is electron concentration, and ξ is electric field. Hole current is defined as [11]

$$J_p = q(n\mu_p\xi - D_p\nabla p), \tag{3}$$

where μ_p is hole mobility, D_p is the hole diffusion coefficient, and p is hole concentration.

Continuity Equations

Each type of carrier actions changes the carrier concentration with time. The combined effect of these actions is governed by continuity equations. The electron continuity equation is defined as [11]

$$\nabla \cdot \frac{J_n}{q} - R_{GR} = 0, \tag{4}$$

where J_n is electron current and R_{GR} is the recombination rate defined as [11]

$$R_{GR} = \frac{np - n_i^2}{\tau_p(n + n_t) + \tau_n(p + p_t)}, \tag{5}$$

where τ_n is electron lifetime, τ_p is hole lifetime, n_t is trap induced electron concentration, p_t is trap induced hole concentration, and n_i is intrinsic carrier concentration. The hole continuity equation is defined as [11]

$$\nabla \cdot \frac{J_p}{q} + R_{GR} = 0, \tag{6}$$

where J_p is hole current.

Carrier Mobilities

Vydyanath reported electron mobilities of several thin films grown by MBE.[16] At a temperature of $80°K$, electron mobility is $4.5E4\,cm^2/VS$ for $Hg_{0.768}Cd_{0.232}Te$ and $1.6E5\,cm^2/VS$ for $Hg_{0.800}Cd_{0.200}Te$. Hole mobility is typically approximately 1% of electron mobility. The effective electron mass in CdTe is $m_{eff} = 0.096\,m_e$,[17] where m_e is electron mass. The light electron mass leads to much more quantum effect than normal electron's.[16] In an infinite deep potential well, the mth energy level is $E_m \propto 1/m_{eff}$.[18] The electron mobility is thus proportional to $1/m_{eff}$. In triangular 2DEG, E_m is proportional to $m_{eff}^{-1/3}$.[4] Likewise, the electron mobility is proportional to $m_{eff}^{-2/3}$. Ali showed a relationship between electron mobility and sheet charge density in a 2DEG channel.[4] The electron mobility at temperature $77°K$ can be modeled as

$$\mu_n = -2.35511\times10^7 + 1.71355\times10^6\ln\theta - 3.11170\times10^4(\ln\theta)^2, \tag{7}$$

where θ is sheet charge density measured in cm^{-2} and μ_n is electron mobility measured in cm^2/Vs.

Carrier Lifetimes

Carrier lifetimes depend on the Cd composition fraction, temperature, traps, doping concentrations, donor types, annealing processes, and recombination types. Edwall et al. reported carrier lifetimes for different Cd composition fractions.[20] At $80\ °K$, electron lifetime is approximately $0.5\,\mu s$ for $Hg_{0.768}Cd_{0.232}Te$ with electron concentration between $2E14$ and $2E15\ (cm^{-3})$. Hole lifetime is typically 1% of an electron's. In a 2DEG channel, background noise in doping concentration less than $1.0E14\,cm^{-3}$ can be neglected because the high electron concentration screens the impurity-generated electric field.[4,21] As observed from device simulations, carrier concentration in the channel well exceeded the limit. Therefore, carrier lifetimes in 2DEG were

long in the computational analysis.

Pseudomorphic Channel

Simulation for a 2DEG quantum well device requires constructing quantum wave functions. Accurate computation is difficult and computation time is very long if a large amount of wave functions are taken into consideration. In a PHEMT device, it is convenient to consider the 2DEG channel as a modified classic channel. Acceleration of electron mobility in a pseudomorphic channel results from mismatched crystal strain.[22] Hence, computer simulations for PHEMT can still be valid if channel parameters such as carrier mobility and lifetimes in the pseudomorphic layer are properly modified. Electron current equation in the 2DEG channel is defined as

$$J_n = \Theta_n \eta_n q n \mu_n \xi, \tag{8}$$

where Θ_n is the modulus coefficient of electron mobility and η_n is the modulus coefficient of electron concentration. As discussed previously, electron mobility increased due to lattice strain. Θ_n was thus considered greater than one. Jaffe et al. observed that change of electron concentration in 2DEG was fairly insignificant in a lattice-matched InGaAs channel.[23] This may be explained by using Weisbush's calculations.[24] DOS (density of states) of a triangular 2DEG of a given energy is proportional to m_{eff} times the number of m of different k_z states at that energy. $k_z = m\pi / L$ and L is the width of an infinitely deep well. DOS is a factor in calculating electron concentration,[16] which, involving η_n, depends of effective electron mass and the potential well.

Small Signal Analysis

Transconductance in the active region can be obtained by using [11]

$$g_m = \frac{dI_D}{dV_G}, \tag{9}$$

where I_D is drain current and V_G is bias voltage on a gate. The transistor capacitance can be modeled as [11]

$$C_t \cong C_{gs} + C_{gd} + C_{gss}, \tag{10}$$

where C_t is total capacitance, C_{gs} is gate-source capacitance, C_{gd} is gate-drain capacitance, and C_{gss} is gate-substrate capacitance. The transition frequency can be obtained by using [11]

$$f_T = \frac{g_m}{2\pi C_t} \tag{11}$$

Substantiation for Model Equations

The device was analyzed by using the finite element method. To verify accuracy of the simulation approach, a device fabricated by Dewames et al. was computed.[26] R_0A of the device was calculated over different temperatures. The computer simulation indicated *10%* accuracy in a temperature range between *200-300°K*. With proper carrier mobilities applied, the simulation also correctly predicted a flat-tailed effect of R_0A at low temperatures.[1]

Computer Simulation Results and Discussions

Device Simulations

The device shown in Figure 2 was operated at *80 °K*. Under such conditions, thermal noise was significantly reduced. Traps were located at midgaps. The source and substrate were grounded. Those results are featured in Section 8. Figure 3 is the valence band diagram. Figure 4 is the conduction band diagram. Figure 5 is the band diagram viewed at a gate cross-section. Figure 6 is the electron concentration, and Figure 7 is the hole concentration.

By using Θ_n = 10.0 and η_n = 1.0, the calculated g_m is approximately $1000\,mS/mm$ and f_T is over *300* GHz. The DOS of HgCdTe in the conduction band is typically $1.0E15\,cm^{-3}$ in such conditions.[25] Observed from digital simulations (not shown), the electron concentration in the pseudomorphic channel was approximately $5.0E16\,cm^{-3}$, higher than typical DOS. The number of

electrons were raised by simply increasing doping concentration in the n region. This provides evidence that electron mobility was elevated in the channel.

Other issues must be considered. In this device, the heterojunction and electrical junctions are abrupt, whereas in reality the junctions are usually graded. This can diminish the built-in electric field across junctions. The intrinsic field may still be intense after impairment. Carrier tunneling probability is significantly increased under such conditions.[25] Weishush stated that strain-layer pseudomorphic AlGaAs/GaInAs split the valence band, cause it to raise. The distortion effect in bandgap properties may also be true for HgCdTe and requires further study.

Applications

For MMIC applications, power dissipation is a major concern in designing the number of transistors per unit area. Existent HEMTs generally possesses low noise figures. The minimum noise figure is proportional to I_{ds}/g_m^2 where I_{ds} is drain-source current.[28] HgCdTe PHEMT is also likely to inherit this property, and due to high g_m, the noise figure is low. From Equation 11, f_T is proportional to g_m. High transconductance also contributes to high transition frequency. In a sufficient high frequency and low temperature, power consumption for a pure metal with low resistivity such as Al, Cu, Ag, or Au is very low.[29] High g_m, f_T, and a low noise figure at low current levels help cut down power consumption while maintaining high digital performance. In addition, the specific heat (measured in J/KgK) of Si at room temperature is *702* whereas that of coloradoite is *164*. A system with high specific heat is also a good heat reservoir.[30] Due to the properties of HgCdTe, device packing density of MCT HEMT IC (integrated circuits) could be made higher than that of Si IC. Thermal conductivity of $Hg_{1-x}Cd_xTe$ is less than that of GaAs or Si. This can cause a heating problem. However, the generated heat in a electron device can be dissipated when operating at a high frequency.[29]

In many cases, particle diffusion coefficient (D) in solids can be predicted by the Arrhenius equation[31]

$$D = D_0 e^{-Q/kT}, \tag{12}$$

where D_0 is frequency factor measured in cm^2/s, Q is activation energy measured in eV, k is Boltzmanns constant, and T is temperature. D_0 of Cd in Coloradoite is *3.1E-4* with Q = 0.66 measured by using radioactive method at *250-350°C*.[32] D_0 of Al in GaAs is *1.0E-14* with Q = 4.3 measured by using AES (Auger Electron Spectroscopy) in temperature ranges of *850-1100°C*.[33] By using MBE, growth temperature of GaInAs or AlInAs is in a range between *600-700°C*.[4] Due to the lower temperature property, technologies used for manufacturing HgCdTe devices may be simpler than those for GaInAs or AlGaAs. Fabrication cost of $Hg_{1-x}Cd_xTe$ material can thus be lower than that of AlGaAs. In MIC (microwave integrate circuits), interconnection structures such as microstrips and co-planars, which generally use aluminum, copper, silver, or gold as conductor materials, must be considered among devices.[29] In comparison, D_0 of Cu in CdTe is *8.2E-8* with Q = 0.64 measured by using IB (Ion Backscattering method) in a temperature range of *290-350°C*.[34] D_0 of Cu in Si is *4.7E-3* with Q = 0.43 measured by using RM (Radioactive Method) in temperature ranges between *300-700°C*.[35] D_0 of Cu in GaAs is *3.0E-2* with Q = 0.53 measured by using RM in a temperature range of *100-500°C*.[35] Cu appears to be more stable in CdTe than in Si or GaAs.

Strength of chemical bond ($\aleph$ measured in kJ/mol) is energy change of a reaction in which the following bond is broken: $AB \rightarrow A + B$, where AB is a compound of A and B. At room temperature, $\aleph$ of AlAl is *133*, $\aleph$ of AlAs is *202*, $\aleph$ of CdTe is *100*, and $\aleph$ of HgTe is less than *142*, $\aleph$ of CuGa is *215*, $\aleph$ of CuCu is *176*, and $\aleph$ of CuTe is *278.7*.[38-43] For lattice structures, Si is of a diamond structure, HgCdTe and AlGaAs are zinc-blended, and Al and Cu are FCC.[36]

HgCdTe may provide not only an alternative for existent PHEMT materials, but also reduce fabrication cost and time in MMIC applications.

Acknowledgments

The theoretical development of HgCdTe devices was supported in part of SBIR contracts with Army Night Vision & Electronic Sensors Directorate, Army Research Lab, and AET, Inc..[37] The authors would like to acknowledge Dr. Glenn Hess, G. Newsome, and T. Fischer for technical assistance. The authors also thank Dale Means for solving computer problems in the early development stages of the MCTS computer model.

References

1 Hung-ming Dai; Adaptive FEM Based Numerical Simulation of Two-Dimensional Hg(1-x)Cd(x)Te Heterojunction Photovoltaic Detectors; Florida Institute of Technology; 2000

2 Hess, Glenn T., Sanders, Thomas J., Dai, Hang-Ming, Newson, Gwendolyn, Fischer, Theodore; "3D focal plane array modeling for IRFPA process operation, and performance simulations"; Proceedings of SPIE, Vol. 3063, pp. 50-9, Infrared Imaging Systems: Design, Analysis, Modeling, and Testing VIII, Gerald C. Holst; 1997

3 Hess, Glenn T., Sanders, Thomas J., Dai, Hang-Ming, Newson, Gwendolyn, Fischer, Theodore; "Heterojunction Model for Focal Plane Array Detector Devices"; University/Government/Industry Microelectronics Symposium, Rochester Institute of Technology, pp. 128-32; 1997 IEEE.

4 Fazal Ali, Aditya Gupta; HEMTs & HBTs: Devices, Fabrication, and Circuits; Artech House, Boston Longon; 1991

5 J. K. Abrokwah et al.; "High performance self-aligned (Al, Ga) As/(In, Ga)As pseudomorphic HIGFET's"; IEEE Electron Device Lett.; EDL-10, 225; 1989

6 P.C. Chao et al.; "V- and W-Band power and low-noise HEMT's; Extended Abstract 21st Conf."; Solid State Devices and Materials, Tokyo, 225; 1989

7 A. W. Swanson; "The pseudomorphic HEMT", Microwave & RF, 645; 1986

8 J. W. Mathews and A. E. Blakeslee; "Defects in epitaxial multi-layers, (I.) Misfit dislocations"; J. Crystal Grow; vol. 27, 118; 1974

9 Ferry, Dave K.; Gallium Arsenide Technology; Sams of McMilan, Howard W. Sams & Co., Indianapolis; 1985

10 Schmit, J. L. and E. L. Stelzer; "Temperature and Alloy Compositional Dependences of Energy Gap of $Hg_{1-x}Cd_xTe$ ", J. Appl. Physics, 40, 4865; 1970

11 Yang, Edward S.; Microelectronic Devices; McGraw-Hill; 1988

12 S. Liiu, M.B. Das et al.; "Low frequency noise behavior of InGaAs quantum well structured MODFET's from e-2 to e8 Hz", IEEE Trans. Electron Devices, vol. ED-33, pp. 576-81; 1986

13 D. D. Edwall, M. Zandian, A.C. Chen, and J. M. Arias; "Improving Material Characteristics and Reproducibility of MBE HgCdTe", J. of Elec. Mat., Vol. 26, No. 6, pp. 493-501; 1997

14 S. M. Liu et al; "Determination of 2-D electron gas carrier mobility in short gate length MODFET's by direct elimination of parasitic resistance effects"; IEEE Electron Device Lett., vol. EDL-6, pp. 594-6; 1985

15 S. Kuroda et al.; "A new fabrication technology for AlGaAs/GaAs HEMT LSIs using InGaAs nonalloyed ohmic contacts"; IEEE Trans. Electron Devices, Vol. EDL-36, 2196; 1986

16 H. R. Vydyanath et al.; "Observation of Prevalence of Quasi-Equilibrium in the MBE Growth of $Hg_{1-x}Cd_xTe$ ", J. Elec. Mat., Vol. 27, No. 6, pp. 507-9; 1998

17 Michael Shur; Physics of Semiconductor Devices; Prentice Hall; 1990

18 Richard L. Liboff; Introductory Quantum Mechanics, 2nd edition, 92; Addison Wesley; 1992

19 S. Hiyamizu et al.; "Improved electron mobility higher than 1.0×10^6 $cm^2/V\cdot s$ in selectively doped GaAs/n-AlGaAs Heterostructure grown by MBE", Japan J. Appl. Physics, vol. 22., pp. 606-11; 1983

20 Edwall, D.D., DeWames, R.E., Mclevige, W.V., Paski, J.G., and Arias, J.M.; "Measurement of Minority Carrier Lifetime in ntype, MBE, HgCdTe and Its Dependence on Annealing"; J. Elec. Mat. Vol. 27, No.6, pp. 698-702; 1998

21 Neil W. Ashcroft and N. David Mermin; Solid State Physics, pp. 337-51; Saunders College, Philadelphia; 1976

22 J.W. Matthews and A.E. Blakeslee; "Defects in epitaxial multi-layers. I. Misfit dislocations", J. Crystal Grow., vol. 27, 118; 1974

23 M.D. Jaffe, at. el.; "Cornell Conference on Advanced Concepts in High Speed Semiconductor Devices and Circuits"; 1987 Proceedings IEEE; Cornel University. Ithaca, NY; 1987

24 Claude Weisbush Borge Winter; Quantum Semiconductor Structures, pp. 20-1; Academic Press, Inc.; 1991

25 Sze, S. M.; Physics of Semiconductor Devices, 2nd edition; Wiley, New York; 1981

26 Dewames, R.E et al.; "Dark Current Generating Mechanism in Short Wavelength Infrared Photovoltaic Detectors"; Journal of Electronic Materials, Vol. 27, No. 6, pp. 722-6; 1998.

27 Peter A. Rizzi; "Microwave Engineering Passive Circuit", 43; Prentice Hall; 1988

28 K. H. G. Duh et al.; "Ultra-low noise characteristics of millimeter-wave high electron mobility transistors"; IEEE Electron Device Lett. vol. EDL-9, 521; 1988

29 Samuel Y. Liao; Microwave Device and Circuits, second edition; The Southeast Book Company; 1985

30 Salinger and Sears; Thermodynamics, Kinetic Theory, and Statistical Thermodynamics, Third Edition, 83; AdddisonWesley Publishing Company; 1986

31 S. Wolf and R.N. Tauber; Silicon Processing for the VLSI Era, Volume 1 -- Process Technology, 649; Lattice Press; 1986
32 V. V. Belov, F. A. Zaitov, and G. E. Popovyan; Sov. Physics Solid State, 11, 1627; 1970
33 L. L. Chang and A. Koma; Appl. Physics Letter, 29, 138; 1976
34 H. Mann, G. Linker, and O. Meyer; Solid State Comm., 11, 475; 1972
35 R.N. Hall and J.H. Racette; J. Appl. Physics, 25, 379; 1964
36 Neil W. Ashcroft and N. David Mermin; Solid State Physics, pp. 284-98; Saunders College, Philadelphia; 1976
37 Florida Institute of Technology and Advanced Engineering Technology (AET) Inc.; Small Business Innovation Research (SBIR) Program: "3D Model of Advanced FPA Detector with Statistical Results Presentation"; NVESD, US Army CECOM and Army Reserch Lab., Phases I and II, A96081; 1997-1999
38 Z. Fu, G. W. Lemire, G. A. Bishea, and M. D. Morse; J. Chem. Physics; 93, 8420; 1990
39 V. Piacente and G. Balducci; Dyn. Mass Spectrom, 4, 295; 1976
40 M. Grade and W. Hirschwald; Phys. Chem., 86, 899; 1982
41 V. N. Kondratiev; Bond Dissociation Energies, Ionization Potentials and Electron Affinities; Mauka Publishing House; 1974
42 M. Carbonel, C. Bergman, and M. Laffite; Colloq. Int. Cent. Nat. Resch. Sci.; 201, 311; 1972
43 E. A. Rohlfing and J. J. Valentine; J. Chem. Phys.; 84, 6560; 1986

Figures

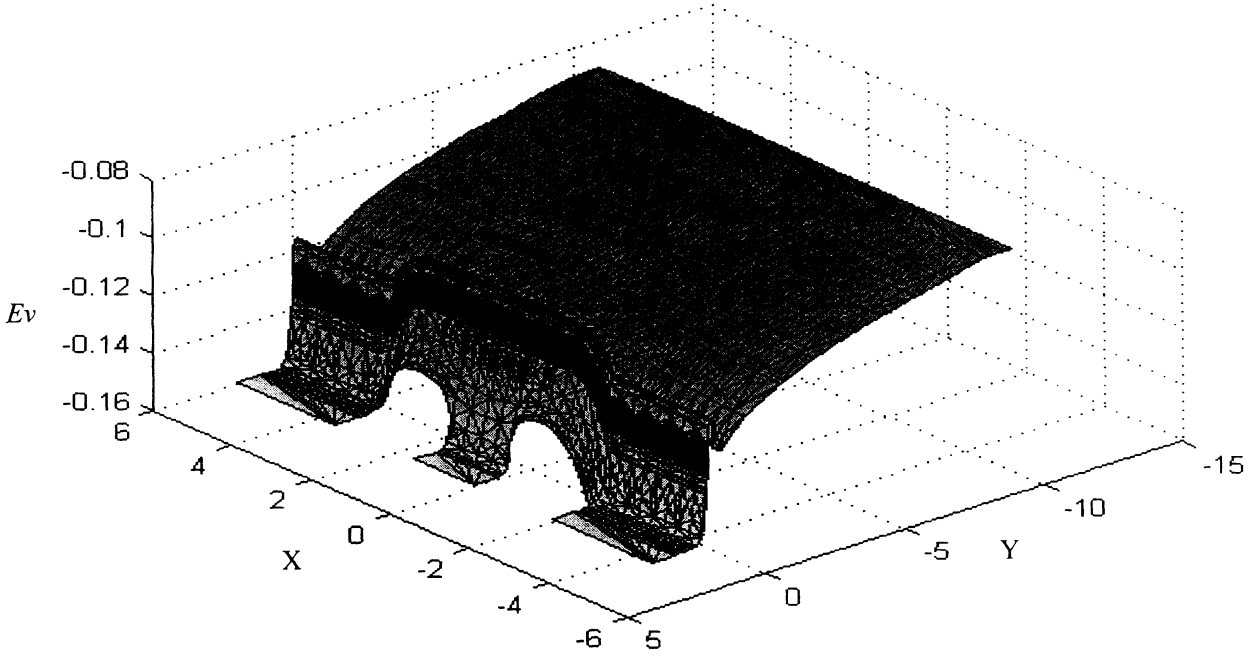

Figure 3 Valence band diagram shown in 3-D

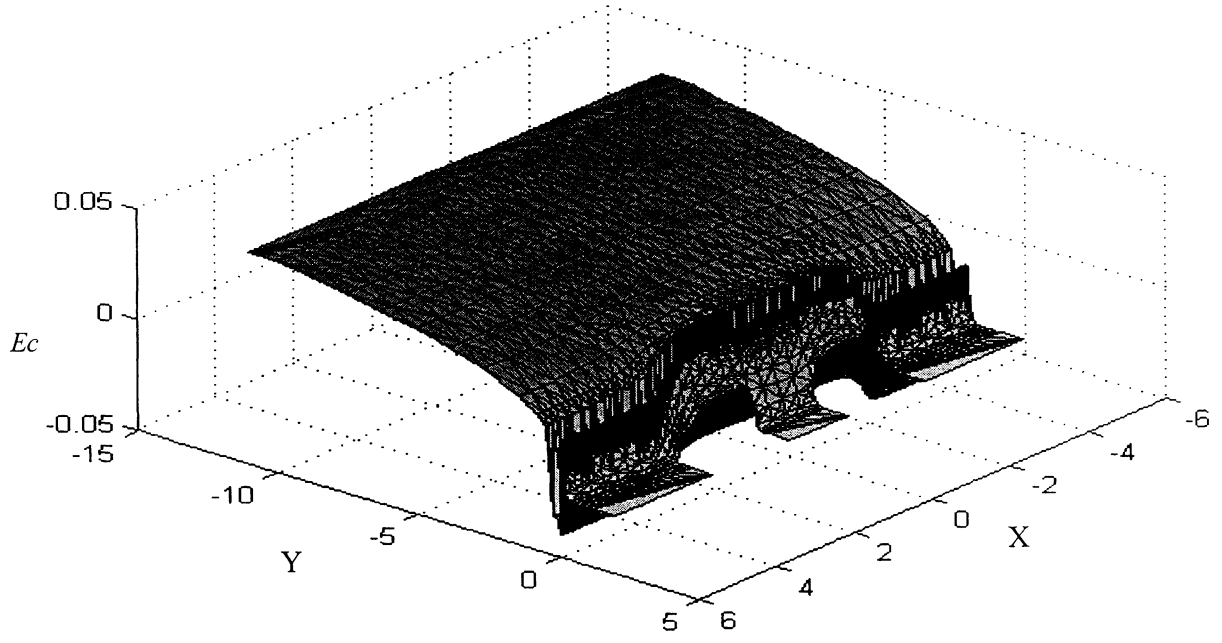

Figure 4 Conduction band diagram shown in 3-D

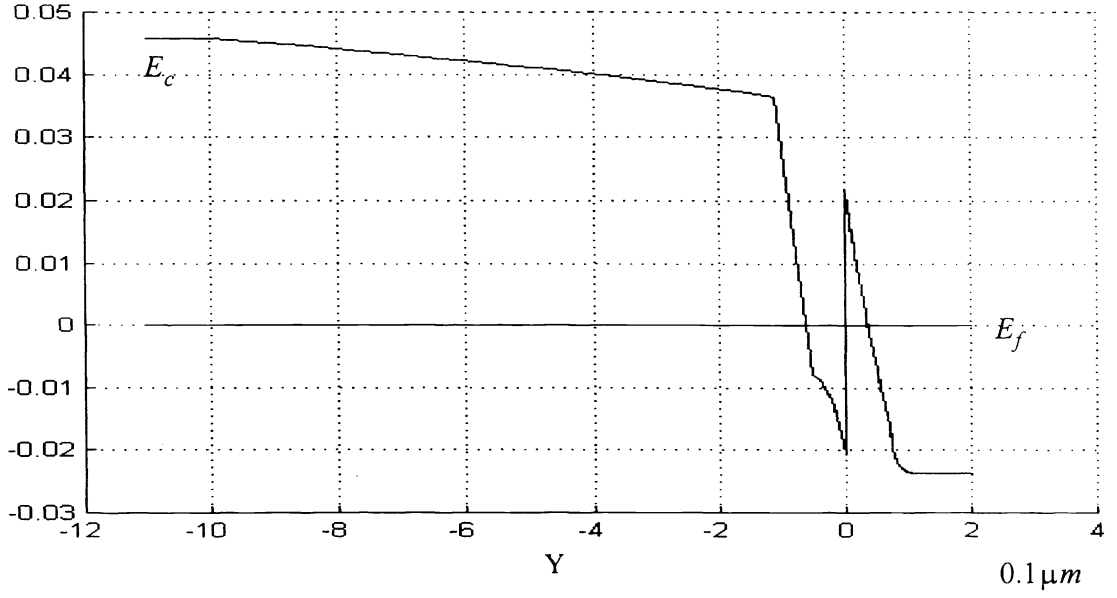

Figure 5 1D simulation for conduction band diagram at cross-section of gate

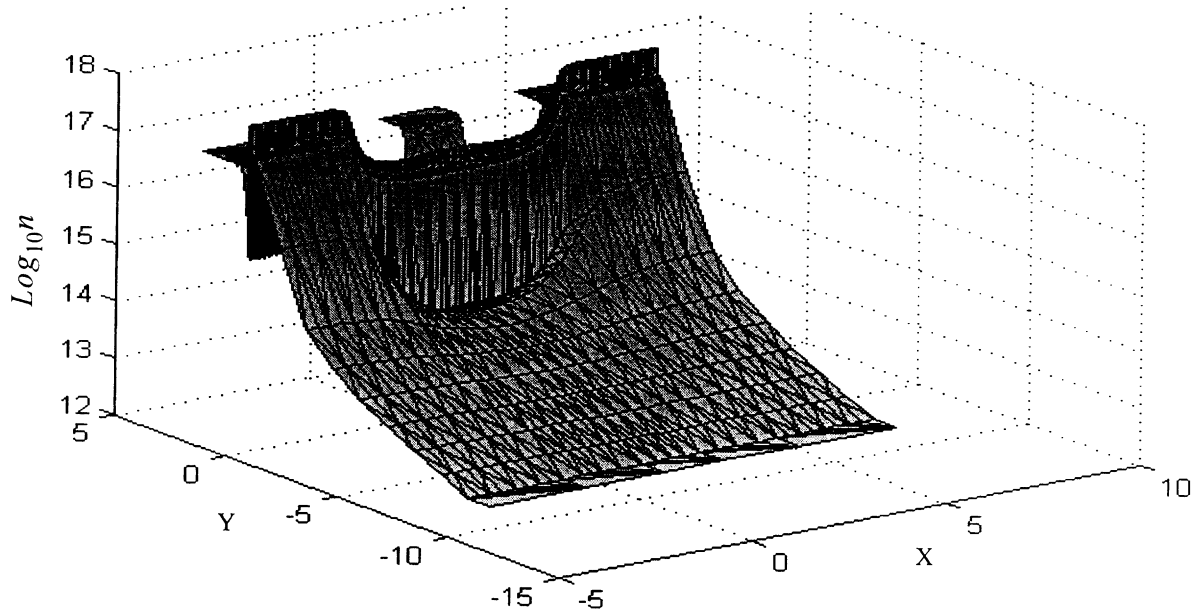

Figure 6 Electron concentration shown in 3-D

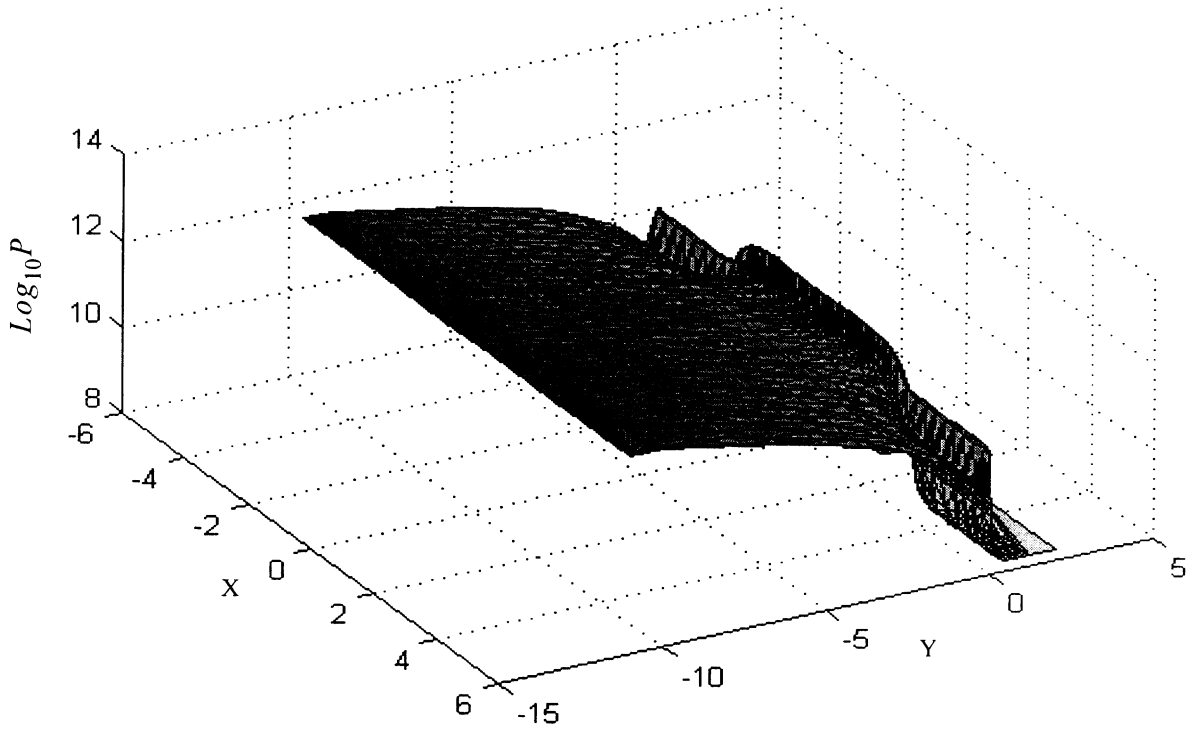

Figure 7 Hole concentration shown in 3-D